START-TO-END SIMULATION OF THE LCLS-II BEAM DELIVERY SYSTEM WITH REAL NUMBER OF ELECTRONS*

J. Qiang#, M. Venturini, C. Mitchell, C. Papadopoulos, LBNL, Berkeley, CA94720, USA
Y. Ding, P. Emma, Z. Huang, G. Marcus, Y. Nosochkov, T. O. Raubenheimer, L. Wang, M. Woodley, SLAC, Menlo Park, CA 94025, USA

Abstract

The LCLS-II as a next generation high repetition rate FEL based X-ray light source will enable significant scientific discoveries. In this paper, we report on progress in the design of the accelerator beam delivery system through start-to-end simulations. We will present simulation results for three charges, 20 pC, 100 pC and 300 pC that are transported through both the hard X-ray beam line and the soft X-ray beam line for FEL radiation.

INTRODUCTION

Next generation high brightness FEL X-ray light sources provide great opportunity for scientific discovery in many fields. The LCLS-II as an upgrade to the current LCLS FEL at SLAC will deliver photons of energy between 200 eV and 5 keV at a repetition rate as high as 1 MHz and is being actively designed under a multi-laboratory collaboration [1]. Figure 1 shows a schematic layout of the LCLS-II beam delivery system [2]. It consists of a high repetition rate photo-injector to generate and accelerate the electron beam to 100 MeV, a laser heater (LH) to suppress microbunching instability, a section of superconducting linac L1 to accelerate the beam to 250 MeV, a bunch compressor BC1, a second section of superconducting linac L2 to accelerate the beam to 1.6 GeV, a bunch compressor BC2, and a third section of superconducting linac L3 to accelerate the beam to 4 GeV, a long bypass transport line, and a magnetic kicker to spread the electron beam to a soft X-ray transport beam line and to a hard X-ray transport beam line. The superconduting linacs in all three sections are made of 1.3 GHz 9 cell superconducting cavities except the two cryomodules of 3.9 GHz third harmonic cavities right before the BC1 to linearize longitudinal phase space.

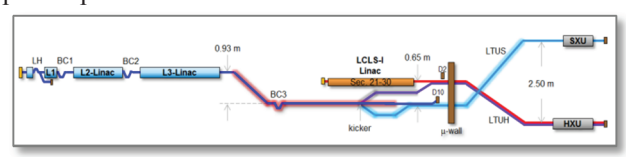

Figure 1: A schematic layout of the LCLS-II.

COMPUTATIONAL SETUP

All simulations presented in this study were done using a 3D parallel beam dynamics simulation framework IMPACT [3-5]. It includes a time-dependent 3D space-charge code module IMPACT-T to simulate photo-electron beam generation and acceleration through the photo RF gun, buncher and boosting cavities, and a position-dependent 3D space-charge code module to simulate electron beam transport through the superconducting linac system. Besides the 3D space-charge effects, the simulation also includes coherent synchrotron radiation (CSR) effects through a bending magnet, incoherent synchrotron radiation inside the bending magnet, RF cavity structure wakefield, and resistive wall wakefield. All simulations were done using the real number of electrons for three bunch charges, 20 pC, 100 pC, and 300 pC, to capture the initial shot noise of the beam, which can have important impact on the final beam quality and FEL performance due to the microbunching instability [6-8]. The total computational time takes from a few hours to about 14 hours on thousands of processors at the NERSC supercomputer center [9].

SIMULATION RESULTS

The simulation starts with an initial particle distribution behind the cathode. The choice of the initial electron beam parameters and the RF gun, the solenoid, the buncher cavity, and the boosting cavities parameters was based on a multi-variable multi-objective optimization [10]. Figure 2 shows the longitudinal phase space distribution and the current profile at the exit of the

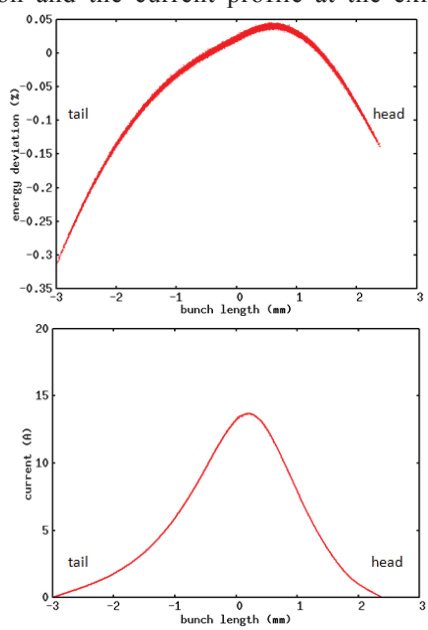

Figure 2: Longitudinal phase space (top) and current profile (bottom) at the exit of the injector.

*Work supported by the Director of the Office of Science of the US Department of Energy under Contract no. DEAC02-05CH11231 and Contract no. DE-AC02-76SF00515.
#jqiang@lbl.gov

ISBN 978-3-95450-134-2

injector for the nominal 100 pC charge case. The relative energy deviation in the longitudinal phase space is small but with noticeable nonlinear component that might affect the final beam compression. The peak current of the beam at this location is about 14 Ampere.

The electron beam coming out of the injector is sent through a laser heater chicane to increase its uncorrelated energy spread to suppress the microbunching instability. A detailed discussion of the microbunching instability in the LCLS-II is presented in the reference [6] of these proceedings. For the nominal 100 pC charge, we assumed a 7 keV increase of uncorrelated energy spread from the laser heater. After the laser heater, the electron beam is transported through the first section of the superconducting linac, the third harmonic linearizer, and the bunch compressor chicane BC1 to boost the beam energy and to increase the peak current. The RF accelerating gradient and the phase used in this section of linac are 12.72 MV/m and -12.7 degree respectively. The accelerating gradient and the phase used in the third harmonic cavity are 11.69 MV/m and -150 degree respectively. The bunch compressor BC1 has a compression factor of 6. The bending angle in this chicane is 0.1028 radian and the R56 of the chicane is 0.055 meters. Figure 3 shows the longitudinal phase space and the current profile after the BC1. The longitudinal phase space looks quite linear. The peak current is about 85 A with noticeable modulation due to the microbunching instability. After the BC1, the beam is further accelerated through the second section of the superconducting linac to 1.6 GeV before entering the second bunch compressor BC2. The accelerating gradient and the phase in this section of linac are 14.51 MV/m and -21 degree respectively. The bending angle in BC2 is 0.043 radian and the R56 of the chicane is 0.0379 m. This provides another compression factor of 8 to the beam.

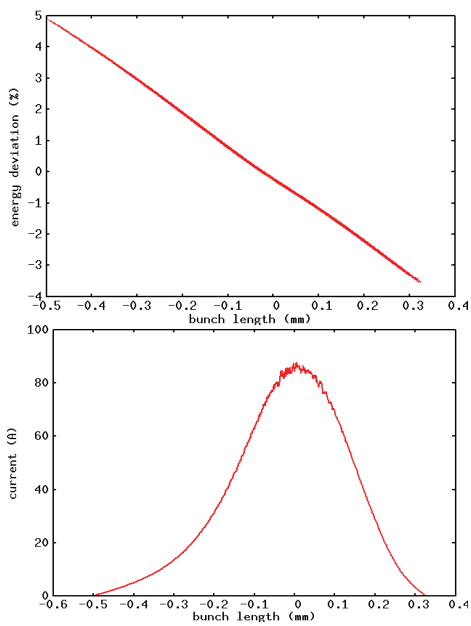

Figure 3: Longitudinal phase space (top) and current profile (bottom) at the exit of the BC1.

Figure 4 shows the longitudinal phase space distribution and the current profile after the BC2. Nonlinear tail forms around both ends of the beam and contributes to two large spikes in the current profile.

After the BC2, the electron beam is further accelerated through the third section of the superconducting linac to reach 4 GeV energy before entering the long transport beam line to the undulator hall. The RF gradient and the phase used in this section of linac are 14.71 MV/m and 0 degree respectively. The long transport beam line consists of a dogleg 1, a long bypass, and a spreader to a soft X-ray transport line and to a hard X-ray transport line. The final longitudinal phase spaces and the current profiles at the entrance to the soft X-ray FEL and the hard X-ray FEL are given in Figs. 5 and 6. Compared with the Fig. 4, the final longitudinal phase distribution becomes flatter and is dechirped by the resistive wakefield through the long transport line. The flat core of the beam is about 13 um with relatively small energy and current modulation due to the microbunching instability. Such a modulation might not present significant impact to the SASE FEL performance but can degrade the performance of the seeded FEL. The current and the energy modulation in the beam at the entrance to the soft X-ray FEL are worse than that at the entrance to the hard X-ray FEL. Study is ongoing to further improve both the soft X-ray and the hard X-ray transport beam lines to minimize the microbunching effects at the entrance to the undulator.

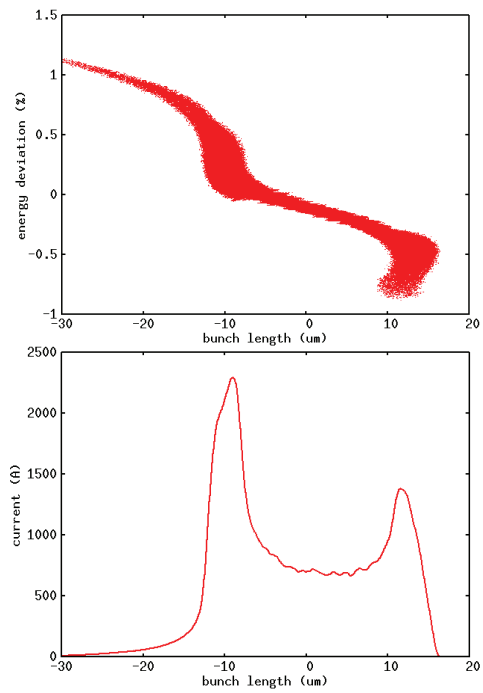

Figure 4: Longitudinal phase space (top) and current profile (bottom) at the exit of the BC2.

Figure 7 shows the transverse projected rms emittance evolution and the transverse center slice emittance (averaged over 5 slices) evolution through the linac and the hard X-ray transport beam line for the nominal 100 pC charge case. Some large spikes in the emittance are due to

ISBN 978-3-95450-134-2

the dispersion inside a chicane or a dogleg. The large projected rms emittance growth after the BC2 and the final dogleg is due to the CSR effects caused by these large current spikes in the beam. Some slice emittance growth is also noticed after the BC1 due to the nonlinear space-charge effects associated with the lattice mismatch and the strong focusing of the beam around this region. The final slice emittances in both horizontal (X) and veritical (X) planes are below 0.5 um. The projected X emittance is about 1um and the projected Y emittance is about 0.5 um.

Besides the nominal 100 pC charge case, we also carried out start-to-end simulation using the real number of electrons for the 300 pC charge and the 20 pC charge. Figure 8 shows the final longitudinal phase space and current profile at the entrance to the hard X-ray FEL for the 300 pC charge. The core of the beam has about 60 um relatively flat distribution with a current beyond 800 A. The final projected transverse emittance is about 1.3 um

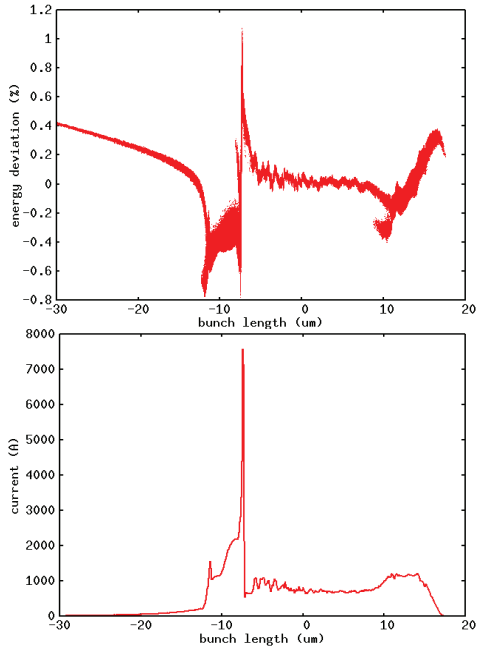

Figure 5: Longitudinal phase space (top) and current profile (bottom) at the entrance to the hard X-ray FEL.

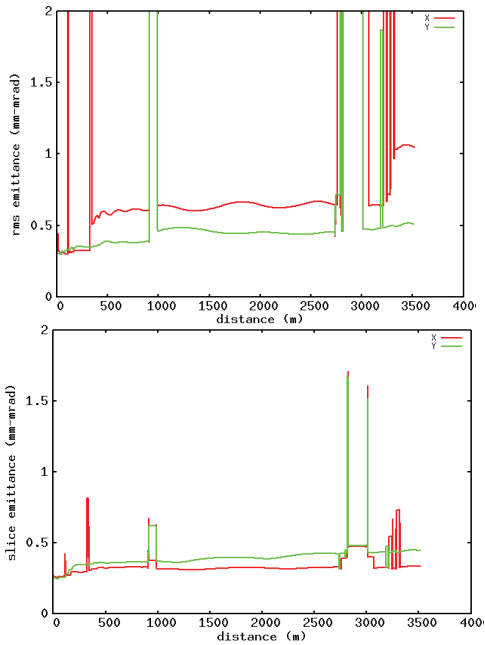

Figure 7: Transverse projected RMS emittance evolution (top) and slice emittance evolution (bottom) through the hard X-ray beam delivery system.

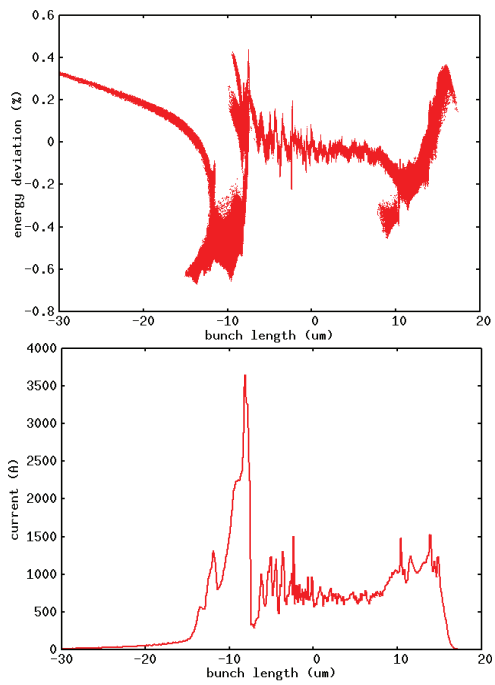

Figure 6: Longitudinal phase space (top) and current profile (bottom) at the entrance to the soft X-ray FEL.

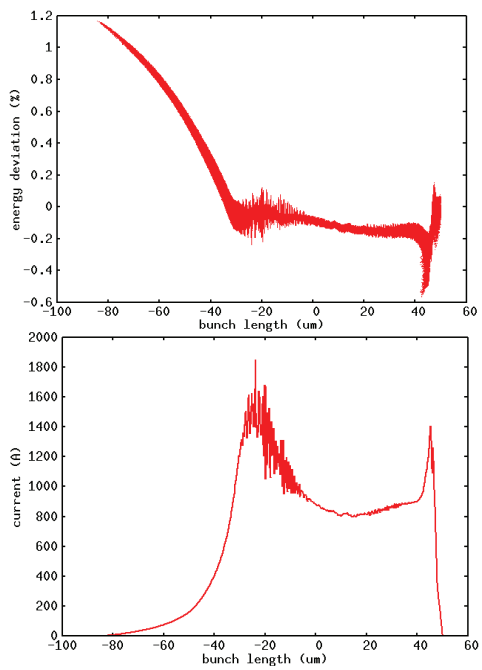

Figure 8: Final longitudinal phase space (top) and current profile (bottom) for the hard X-ray FEL with 300 pC.

ISBN 978-3-95450-134-2

in X and 0.94 um in Y. The center slice emittance is about 0.63 um in X and 0.59 um in Y. Similar phase space distribution and current profile are also obtained for the beam through the soft X-ray transport line.

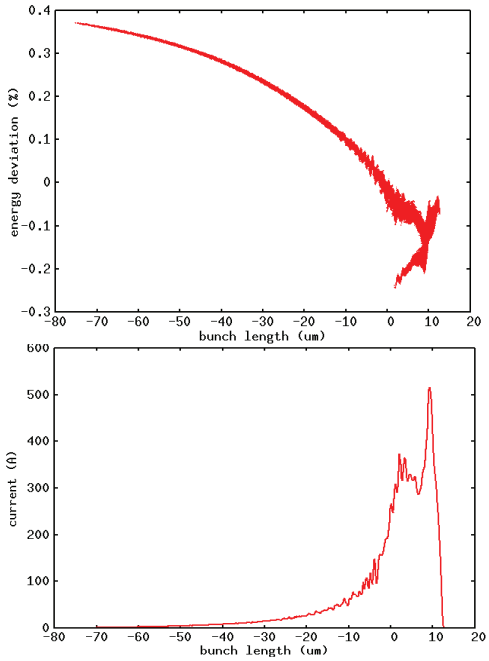

Figure 9: Final longitudinal phase space (top) and current profile (bottom) for the hard X-ray FEL with 20 pC.

Figure 9 shows the final longitudinal phase space and the current profile at the entrance to the hard X-ray FEL for the 20 pC charge case. The peak current in the core of the distribution is about 300 A with a length of about 9 um. The final projected rms emittances are 0.21 um in X and 0.13 in X. The center slice emittances are 0.13 um and 0.12 um in X and Y planes respectively.

SUMMARY AND DISCUSSIONS

As a summary, Table 1 gives some final beam parameters at the entrance to both the hard X-ray FEL (blue) and the soft X-ray FEL (brown) from the start-to-end simulations using real number of electrons. Those parameters that are important to the FEL performance include peak current inside the core, uncorrelated energy spread inside the core, total projected transverse RMS emittances, and core slice emittances. The 300 pC charge gives the largest ~900 A peak current inside the core of the beam. The nominal 100 pC charge leads to a final ~750 A peak current, and the 20 pC charge produces ~300 A peak current inside the core of the beam. The final transverse core slice emittances are below 1 um for all three charges. The total projected RMS emttiances are around 1 um for 100 pC and 300 pC charges except the one with 100 pC charge after the soft X-ray beam line. This large total projected emittance is due to the large fish tail shape distribution in the longitudinal-horizontal plane around the tail of the beam where a large energy tail is also observed in the top plot of the Fig. 6. This part of the beam might not contribute to the desired FEL radiation from the core of the beam in the downstream undulator. The final uncorrelated rms energy spread is below 600 keV for all three bunch charges.

Table 1: Final Beam Parameters at the Entrance to the Hard X-ray FEL (blue) and the Soft X-ray FEL (brown)

IMPACT Studies	I_peak (A)	σ_E (keV)	Proj. ε_x / ε_y (mm-mrad)	Slice ε_x / ε_y (mm-mrad)
20 pC	299	446	0.21 / 0.13	0.16 / 0.10
	294	444	0.23 / 0.12	0.15 / 0.10
100 pC	760	480	1.05 / 0.51	0.34 / 0.43
	755	592	3.5 / 0.44	0.34 / 0.42
300 pC	892	468	1.28 / 0.94	0.64/ 0.52
	921	529	1.21 / 0.90	0.56 / 0.53

The electron beam quality parameters listed in the Table 1 result in a reasonable FEL performance in the downstream undulators[7]. Further improvement to the quality of the beam is still undergoing. For example, recently, we have optimized the settings of the compensation chicane to further reduce the microbunching instability effects through the long transport line. We are also working on improving the beam current profile and reducing the microbunching effects by using a third bunch compressor right before the spreader. This bunch compressor helps to lower the compression factor needed in the first two stages and the peak current through the long bypass, which in principle will reduce the growth of the microbunching instability. This bunch compressor was used in the 20 pC charge case presented here. The challenge with this delayed compression is to remove the longitudinal energy chirp in the final beam distribution since the distance to the undulator entrance is short and the resistive wall wakefield might not be large enough to remove the energy chirp. Besides improving the longitudinal energy/density profile, we are also working on understanding the transverse emittance growth in the linac.

REFERENCES

[1] T. O. Raubenheimer, "Technical challenges of the LCLS-II CW X-ray FEL," in proceedings of IPAC2015, Richmod, VA, USA.
[2] P. Emma et al., in proceedings of FEL'14, THP025.
[3] J. Qiang et al., PRST-AB 9, 044204 (2006).
[4] J. Qiang et al., J. of Comp. Phys., 163, 434 (2000).
[5] J. Qiang et al., PRST-AB 12, 100702 (2009).
[6] J. Qiang et al., PRST-AB 17, 030701 (2014).
[7] M. Venturini et al., "The microbunching instability and LCLS-II lattice design: lessons learned," in these proceedings.
[8] G. Marcus et al., "High fidelity start-to-end numerical particle simulations and performance studies for LCLS-II," in these proceedings.
[9] http://www.nersc.gov
[10] C. Papadopoulos et al, "RF injector beam dynamics optimization for LCLS-II," SLAC-PUB-16210 (2014).

ISBN 978-3-95450-134-2